



The control of morphology and structure of galvanostatically produced tin dendrites by analysis of chronopotentiometry response

Nebojša D. Nikolić¹ · Jelena D. Lović¹ · Vesna M. Maksimović²

Received: 20 October 2022 / Revised: 9 December 2022 / Accepted: 3 January 2023 / Published online: 12 January 2023
© The Author(s), under exclusive licence to Springer-Verlag GmbH Germany, part of Springer Nature 2023

Abstract

The influence of chronopotentiometry response on the morphology and structure of galvanostatically synthesized tin dendritic particles has been investigated. Sn dendrites were electrodeposited at the current density 1.5 times larger than the limiting diffusion current density (-3 mA cm^{-2}) with various amounts of the electricity (200 and 400 mC), and the obtained morphology and structure of the particles were characterized by SEM and XRD techniques, respectively. The strong effect of the amount of spent electricity on the morphology and structure of the particles was observed, and it is explained by morphological and structural analysis of Sn particles produced potentiostatically at various cathodic potentials selected to be in line with the recorded chronopotentiometry response. The strong correlation among chronopotentiometry response, morphology, and structure of the Sn dendrites was established. The spear-like and the dendrites with prismatic branches possessed the strong (200),(400) preferred orientation, and they were obtained with a chronopotentiometry response of about $-1200 \text{ mV vs. Ag/AgCl}$. The chronopotentiometry responses in the $-1210 \div -1740 \text{ mV vs. Ag/AgCl}$ range caused a formation of the fern-like dendrites with the strong (220),(440) preferred orientation. Based on the obtained results, it follows that the chronopotentiometry analysis represents good diagnostic criteria for obtaining Sn powder particles of desired morphology and structure.

Keywords Tin · Electrolysis · Chronopotentiometry · Morphology · Structure · Dendrites

Introduction

Production of tin powders attracts attention in both scientific and technological communities owing to numerous applications of this powder in various industries. These applications are based on specific features of tin, such as a high electrical conductivity, low electrochemical migration, excellent solderability, high corrosion resistance, nontoxicity, and low material cost [1–3]. The main industries using Sn powders are powder metallurgy, sodium-ion and lithium-ion battery production, electronic industry, and manufacture of tin solder paste [3]. Application of Sn powders in these industries is closely related with shape, i.e., morphology of particles,

whereby the morphology of the particles is dependent on a method applied for the production of powder. As powder, Sn can be obtained by non-electrochemical and electrochemical methods. The atomization [1, 4], chemical reduction [1, 5, 6], cementation [1], various polyol [7, 8] and galvanic displacement [9] processes, and colloidal gas apheron (CGA) formation technology [10] are the most often used non-electrochemical methods, and the particles in the form of spheres, nanorods, and bells are usually formed by these methods.

Electrochemical deposition is the often used method for the production of metal powders with many advantages over non-electrochemical methods. It is an environmentally friendly and relatively cheap method giving powders of high purity and controlled shape and size of the particles [11]. The shape and size of the powder particles are easily controlled by regime and parameters of electrolysis, and are determined by nature of the metals [12]. The potentiostatic regimes of electrolysis are primarily useful in an investigation of mechanism of powder formation, while the galvanostatic regimes are of importance for application in industry. The main parameters having an effect on powder

✉ Nebojša D. Nikolić
nnikolic@tmf.bg.ac.rs; nnikolic@ihm.bg.ac.rs

¹ Department of Electrochemistry, Institute of Chemistry, Technology and Metallurgy, University of Belgrade, Njegoševa 12, Belgrade, Serbia

² Vinča Institute of Nuclear Science – National Institute of the Republic of Serbia, University of Belgrade, Belgrade, Serbia

characteristics are the type and composition of electrolytes, the presence of additional agents in the electrolyte, temperature, electrolysis time, electrolyte stirring, type of working electrode, applied values of cathodic potential, or current density, etc.

Sn in the form of powder can be produced by electrolysis from aqueous [2, 13–22] and non-aqueous electrolytes [23–25], deep eutectic solvent (DES) [3, 26, 27], and ionic liquids [28–31]. With a point of view of kinetic parameters [32], Sn is situated in the group of so-called normal metals, featured by the high values of both the exchange current density and overpotential for hydrogen evolution reaction, and by low melting point. These characteristics of Sn as a metal enable production of Sn powder in whole range of current density and cathodic potential applied. The dendrites of various shapes are the most often shapes of electrolytically produced Sn powder particles [3, 13–15, 21, 26]. Aside from dendrites, grains of regular and irregular shape [2, 16], spongy particles [16], nanowires [24, 30], 3D (three dimensional) foam, or the honeycomb-like structures [17, 18] are also obtained by various electrolysis processes. The shape of obtained particles primarily depends on the above-mentioned parameters and regimes of electrolysis. The common characteristic of production of all above listed irregular (or powdered) forms is their formation in conditions of the diffusion control of the electrodeposition process.

The dendrites of Sn can be obtained by both electrochemical [3, 13–15, 21, 26] and non-electrochemical [9] methods, and thanks to a highly branched morphology, they have very diverse applications. Sn dendrites show outstanding surface enhanced fluorescence, and as such, they are very suitable for application in biomolecule detection and sensor devices [9]. For example, Sn dendrites are used for the detection of rhodamine 6G as probe molecules, and the fluorescence enhancement can reach to 29.81-fold that of a pure Al substrate. As anode material for sodium-based batteries, Sn dendrites show a high specific capacity and excellent cycle performances [14]. In this battery type, Sn dendrites exhibit an excellent structural stability upon sodiation and desodiation. The extremely large electrochemically active surface area makes Sn dendrites very suitable for application in various electrochemical devices [14].

In our recent investigation [33], it was shown that overpotential response played a crucial role in creating of the final shape of Cu dendrites during galvanostatic regime of electrolysis. The overpotential response was regulated by electrolysis time duration, i.e., by the amount of the passed electricity, leading to a formation of novel type of Cu dendrite with globular instead of with sharp tips. Simultaneously, unusual morphology of Sn dendrite, not previously observed in the literature, has been recently obtained by applying the galvanostatic regime of electrolysis [21]. Making analogy with the formation of the Cu dendrites, it is assumed that the cathodic

potential response had a decisive effect in the formation of this Sn dendrite type. Anyway, additional analysis of the effect of the cathodic potential (chronopotentiometry) response on the morphology of the Sn particles is necessary, and it will be one of the main aims of this study. The special attention will be devoted to an investigation of chronopotentiometry response on structural characteristics of Sn dendrites, with the aim to establish the existence of correlation between the morphology and structure of Sn particles.

Experimental

Sn in the form of powder was produced from an alkaline hydroxide solution containing 20 g/L $\text{SnCl}_2 \times 2\text{H}_2\text{O}$ in 250 g/L NaOH by applying the constant regimes of electrolysis. In the galvanostatic electrolysis regime, a current density (j) of -3 mA cm^{-2} was used. The selected cathodic potentials (E) in the potentiostatic regime of electrolysis were -1200 , -1270 , and $-1600 \text{ mV vs. Ag/AgCl}$. Sn was electrodeposited with amounts of the passed electricity (Q) of 200 and 400 mC.

All processes of electrolytic production of Sn particles were performed at the room temperature ($T = 22.0 \pm 0.50 \text{ }^\circ\text{C}$) in three compartment electrochemical cells. The working electrode was Cu of cylindrical shape and the surface area was 0.25 cm^2 , while the counter electrode was Pt wire. Ag/AgCl/3.5 M KCl is used as the reference electrode, and this electrode type is denoted with Ag/AgCl in the further text. The electrolyte for Sn electrolysis was made of p.a. (pro analysis) reagents and the ultra-pure water (Millipore, $18 \text{ M } \Omega \text{ cm}$ resistivity). The experimental procedure for the preparation of Cu working electrode is described elsewhere [21].

The techniques of scanning electron microscopy (SEM) and X-ray diffraction (XRD) were used for the characterization of the morphology and structure of electrolytically synthesized Sn dendritic forms, respectively.

The microscope JEOL JSM-6610LV model was used to characterize Sn dendrites produced on the Cu electrodes by various electrolysis processes.

The structural XRD analysis was done using a Rigaku Ultima IV diffractometer in $25 \div 100 2\theta$ range. For this analysis type, the produced Sn dendrites were removed from the Cu working electrode after finished electrolysis process.

Results and discussion

Morphological analysis

Morphologies of tin deposits electrodeposited at a current density of -3 mA cm^{-2} with amounts of the electricity of 200 and 400 mC are shown in Figs. 1 and 2, respectively.

The amount of the electricity of 200 mC was reached after an electrodeposition time of 266.67 s, while the electrodeposition time for 400 mC amount of electricity was 533.34 s. For an electrolyte containing 20 g/L $\text{SnCl}_2 \times 2\text{H}_2\text{O}$ in 250 g/L NaOH, the applied current density was 1.5 times larger than the limiting diffusion current density, and belonged to zone of rapid increase of the current density with increasing cathodic potential after the end of the plateau of the limiting diffusion current density [21].

At the first sight, it can be noticed that very diverse irregular forms of dendritic character were formed with these amounts of the electricity. Sn dendrites of the fern-like shape composed from stalk and branches are predominantly formed with an amount of the electricity of 200 mC (Fig. 1a–c). Some of dendrites grew from one nucleation center in more directions giving dendrite very branchy appearance (Fig. 1b). As shown in Fig. 1c, branches of the dendrite were developed under the right angle from the stalk. Aside from predominant formation of the fern-like dendrites, rare individual dendrites with the spear-like tips were also formed with this amount of the electricity (Fig. 1d). Another important phenomenon is noticed during Sn electrolysis at this current density. It is hydrogen evolution reaction which occurred parallel to the formation of Sn dendrites. This reaction is identified by the appearance of holes in the electrodeposit, since the holes originated from detached hydrogen bubbles. The holes of various sizes are clearly visible from

Fig. 1 Morphology of Sn dendrites produced by a galvanostatic regime of electrolysis at a current density of -3 mA cm^{-2} with an amount of the electricity (Q) of 200 mC: **a–c** the fern-like dendrites, and **d** dendrite constructed from the spear-like and the fern-like parts. The electrodeposition time: 266.67 s

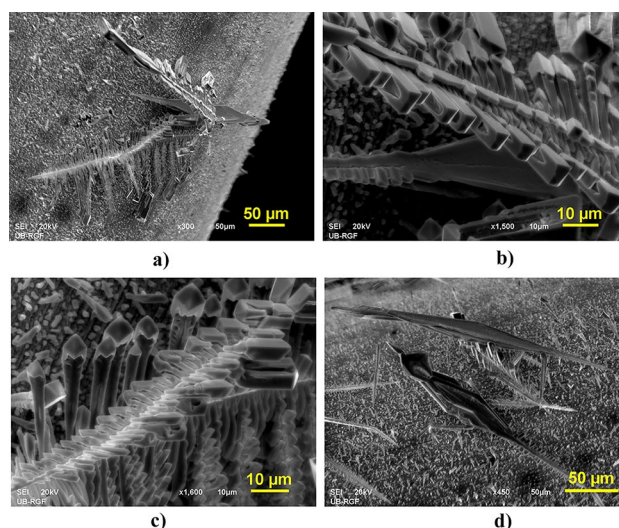
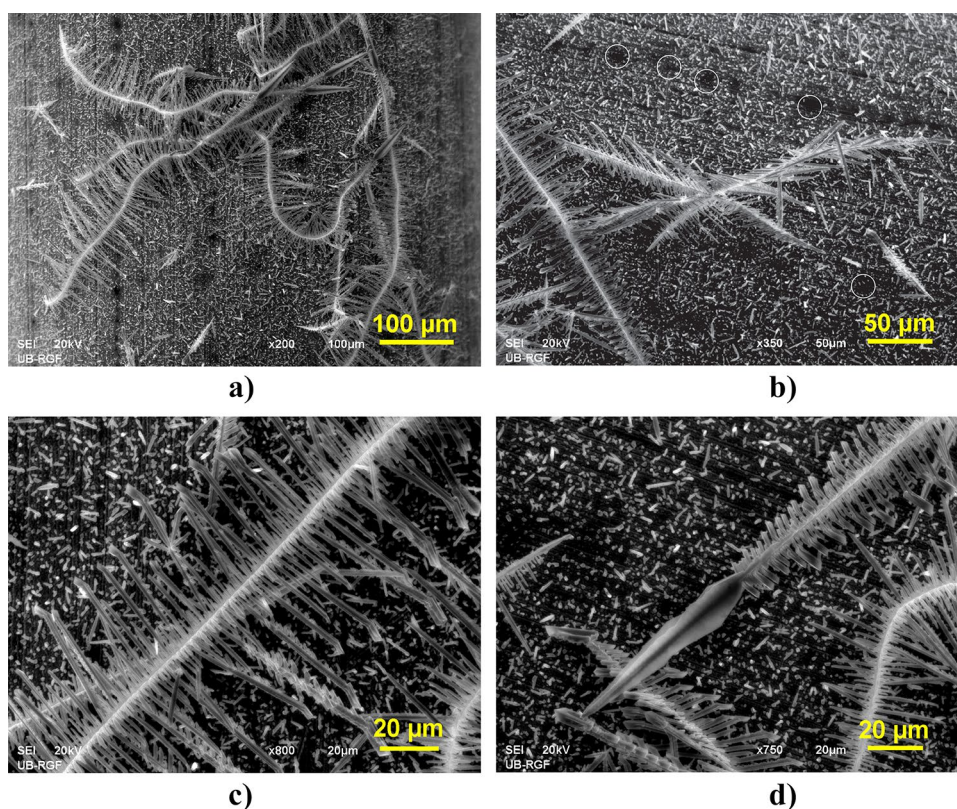


Fig. 2 Morphology of Sn dendrites produced by a galvanostatic regime of electrolysis at a current density of -3 mA cm^{-2} with an amount of the electricity (Q) of 400 mC: **a–c** dendrite with prismatic branches or ends, and **d** dendrite constructed from the spear-like and the fern-like parts. The electrodeposition time: 533.34 s

the surface area of the Sn deposit produced at a current density of -3 mA cm^{-2} with Q of 200 mC (Fig. 1a, b; for example, see parts in circles in Fig. 1b). The presence of hydrogen evolution as the second reaction during Sn electrolysis did

not have any effect on the hydrodynamic conditions in the near-electrode layer, since dendritic growth was not inhibited by the presence of this reaction.

The shape of dendrites obtained at the same current density but with an amount of the electricity of 400 mC (Fig. 2) differed significantly than those obtained with double smaller amount of the electricity. Although the dendritic growth from one nucleation center in more directions is kept (Fig. 2a), the shape of the branches was different from those obtained with the lower amount of the electricity. This dendrite type was constructed from branches of prismatic shape (Fig. 2b), and some tips of the branches had the pyramid-like shape (Fig. 2c). Please note that the dendrite type with the branches of prismatic shape was recently identified as a completely novel type of Sn dendrites [21]. Aside from the 3D dendrites, the spear-like dendrites were also formed with this amount of the electricity (Fig. 2d). In contrast to an amount of the electricity of 200 mC where only tips of the dendrites had the spear-like shape (Fig. 1d), in the Sn dendrites obtained with an amount of the electricity of 400 mC, the larger part of the dendrite had the spear-like shape (Fig. 2d).

The chronopotentiometry technique was applied to explain the formation of various shapes of Sn dendrites. Figure 3 shows the dependence of the cathodic potential response on electrolysis time recorded at a current density of -3 mA cm^{-2} . The overall electrolysis time corresponded to an amount of the electricity of 400 mC, while reached amount of the electricity of 200 mC is denoted by a vertical dash line at this figure. Analysis of the curve revealed that the values of the cathodic potential response were approximately in the $-1210 \div -1740 \text{ mV vs. Ag/AgCl}$ range with an amount of the electricity of 200 mC, whereby the largest part was approximately between -1500 and $-1740 \text{ mV vs. Ag/AgCl}$. The sharp fall of the value of the cathodic potential from -1500 to $-1230 \text{ mV vs. Ag/AgCl}$ occurred between 210 and 220 s of the electrodeposition process. Then, the cathodic potential commenced slowly to fall reaching a value of $-1210 \text{ mV vs. Ag/AgCl}$ after 266.67 s (or 200 mC). Finally, the value of the cathodic potential response was $-1140 \text{ mV vs. Ag/AgCl}$ after passed amount of the electricity of 400 mC. There is another smaller fall in the value of the cathodic potential in a part of the chronopotentiometry curve between 200 and 400 mC passed amount of the electricity. This fall was 62 mV and occurred after 426 s from the beginning of the electrodeposition process.

The three-step form of the chronopotentiometry curve can be explained by the formation and growth of the dendrites during electrodeposition at this current density. The fall of the cathodic potential value is a result of the decrease of the real current density during electrodeposition in the galvanostatic regime [34]. Namely, during the electrodeposition process in this regime, the electrode surface area increases

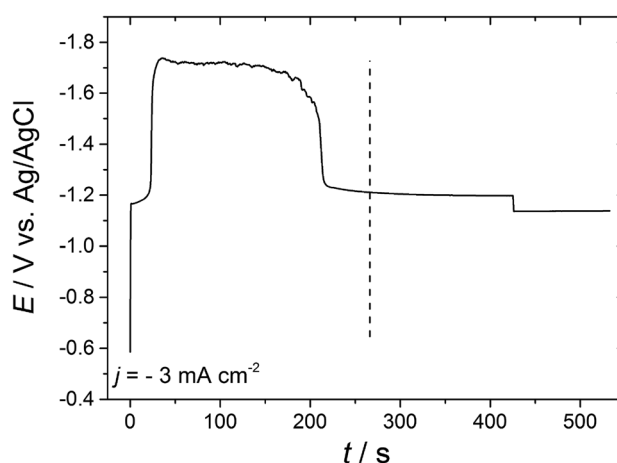


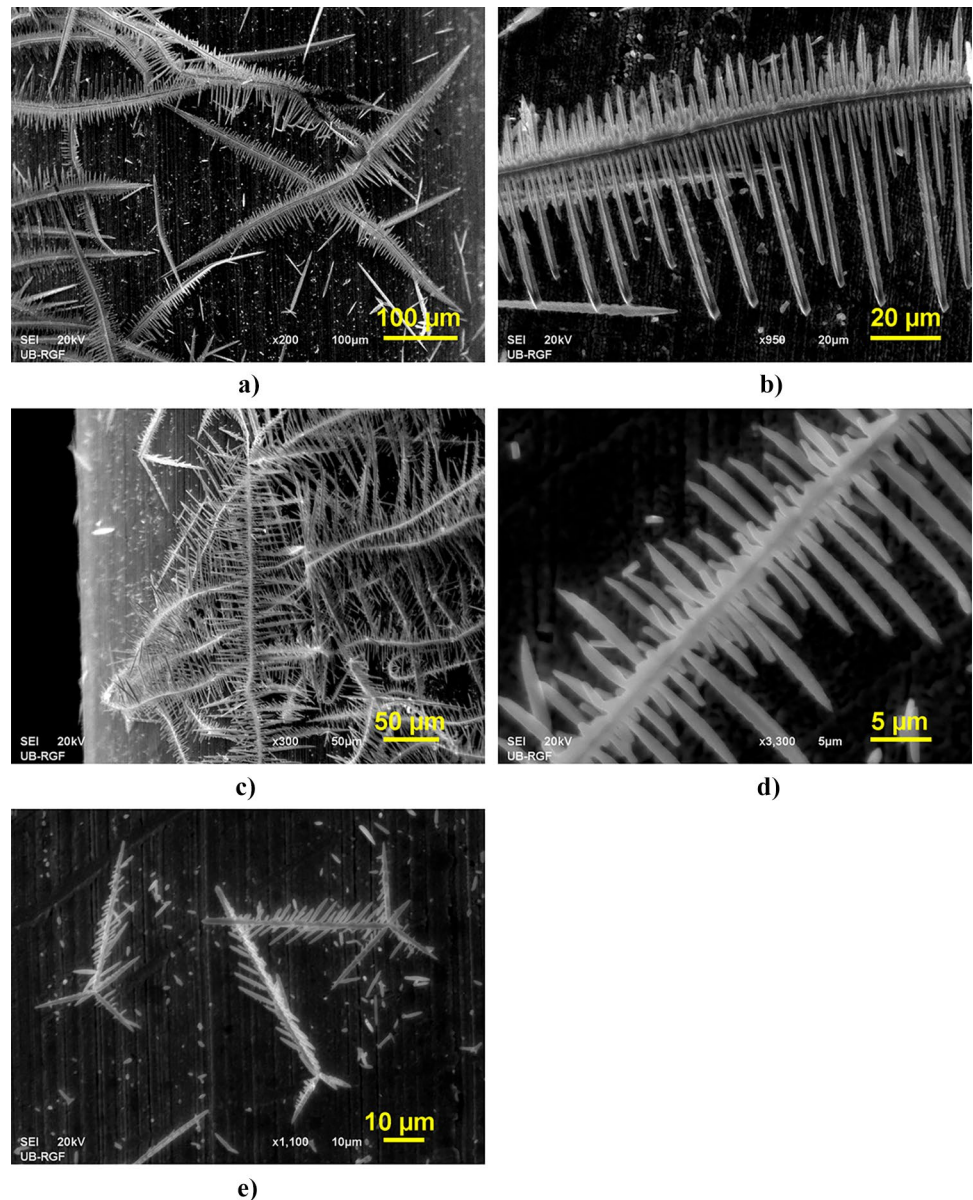
Fig. 3 The chronopotentiometry response obtained during electrolysis process at a current density of -3 mA cm^{-2}

due to the formation and growth of the dendrites, and as a result of it, the real current density decreases.

To examine an influence of chronopotentiometry response on the shape of dendrites, the following morphological analysis was performed. Electrodeposition of Sn was firstly performed by potentiostatic regime of electrolysis at cathodic potentials which belonged to the $-1210 \div -1740 \text{ mV vs. Ag/AgCl}$ range, i.e., up to reached 200 mC amount of the electricity in the galvanostatic regime of electrolysis. Figure 4 shows the Sn deposits potentiostatically produced at cathodic potentials of -1270 (Fig. 4a, b) and $-1600 \text{ mV vs. Ag/AgCl}$ (Fig. 4c–e) with amounts of the electricity of 200 (Fig. 4e) and 400 mC (Fig. 4a–d). The electrodeposition times to reach an amount of the electricity of 400 mC were 417 s at $-1270 \text{ mV vs. Ag/AgCl}$, and 333 s at $-1600 \text{ mV vs. Ag/AgCl}$. At a cathodic potential of $-1600 \text{ mV vs. Ag/AgCl}$, 200 mC amount of the electricity was reached after 240 s. The fern-like dendrites, very similar at the macro level to those obtained by galvanostatically with an amount of the electricity of 200 mC, are formed at both cathodic potentials (Fig. 4a–d). As shown in Fig. 4e, some of dendrites grew from one nucleation center in more directions. This was in line with the morphology of Sn dendrites obtained by the galvanostatic regime of electrolysis with both amounts of the electricity (Figs. 1a, b and 2a). As already mentioned, the growth of Sn dendrites at a current density of -3 mA cm^{-2} also occurred from one nucleation center in more directions, indicating that a mechanism of a dendrite growth is determined by the initial stage of electrolysis (i.e., by nucleation process).

The strong transformation of the shape of galvanostatically synthesized dendrites with an increase of amount of the electricity from 200 to 400 mC, from the dominant fern-like to the dendrites with prismatic ends and the spear-like dendrites, can be explained by the analysis of Sn electrodeposition processes at cathodic potentials belonging

Fig. 4 The fern-like Sn dendrites produced by a potentiostatic regime of electrolysis at cathodic potentials of **a, b** – 1270 mV vs. Ag/AgCl, and **c–e** – 1600 mV vs. Ag/AgCl. The amount of the electricity: **a – d** $Q=400$ mC, and **e** $Q=200$ mC



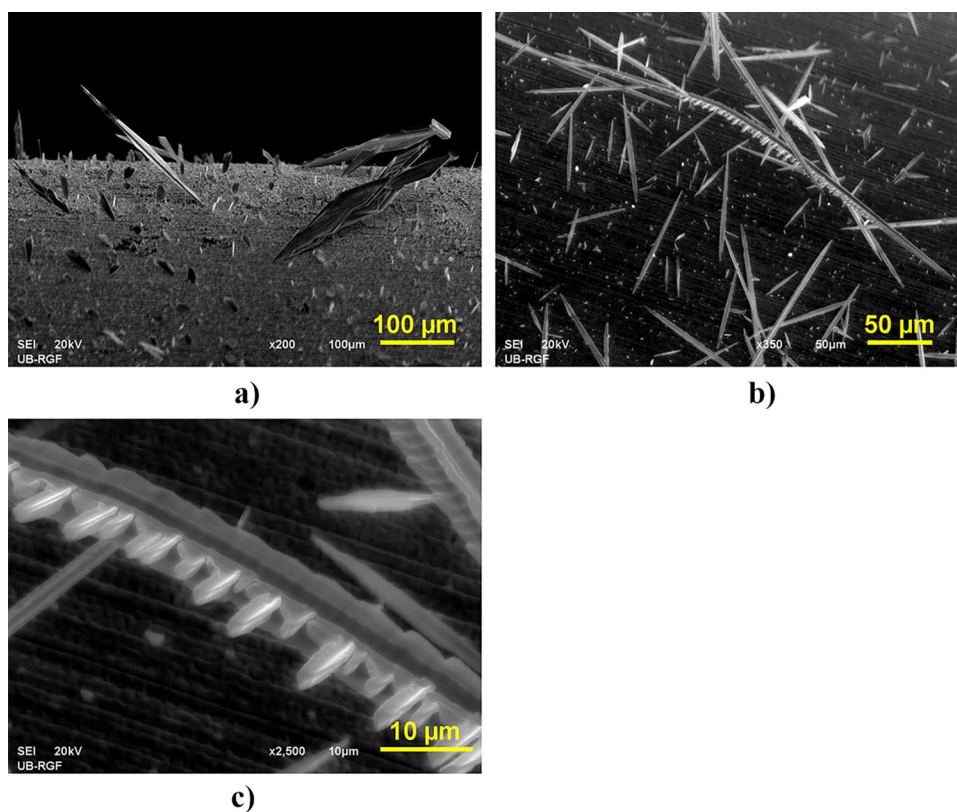
to the $-1140 \div -1210$ mV vs. Ag/AgCl range. Figure 5 shows the morphology of Sn dendrites produced at a cathodic potential of -1200 mV vs. Ag/AgCl with amounts of the electricity of 200 or 400 mC. At a cathodic potential of -1200 mV vs. Ag/AgCl, an amount of the electricity of 200 mC is reached after 287 s, while that of 400 mC was reached after 464 s. As seen from Fig. 5, the spear-like dendrites (Fig. 5a) and the dendrites with prismatic branches (Fig. 5b, c) were obtained at this cathodic potential. It is clear that these morphologies of the dendrites were very similar at the macro level to the galvanostatically synthesized dendrites with spent 400 mC amount of the electricity.

Hence, based on the above morphological analysis of Sn powder forms obtained under various electrolysis conditions, it follows that the final shape of galvanostatically produced

dendrites is determined by the chronopotentiometry response. In this way, it is possible to obtain desired shape of Sn dendrites by simple regulation of length of duration of electrolysis process, i.e., by regulation of an amount of the passed electricity.

One of the best ways to look at an influence of the cathodic potential response on the final shape of dendrites was an analysis of the dendrites composed of the spear-like and the fern-like parts (Figs. 1d and 2d). Although whole dendrite is not shown in Fig. 1d, it is clear that the fern-like part was longer than the spear-like part in the dendrite produced with an amount of the electricity of 200 mC, so that only the tip of dendrite had the spear-like shape. The transformation of dendrite growth from the fern-like to the spear-like shape can be explained as follows: during electro-deposition process with 200 mC amount of the electricity,

Fig. 5 Morphology of Sn dendrites produced by a potentiostatic regime of electrolysis at a cathodic potential of -1200 mV vs. Ag/AgCl: **a** the spear-like dendrite, $Q = 400$ mC; and **b**, **c** a dendrite with prismatic ends, $Q = 200$ mC



the larger part of the electrodeposition process of 266.67 s (i.e., up to 220 s) corresponded to the cathodic potential response between -1230 and -1740 mV vs. Ag/AgCl. As already shown (Fig. 4), the fern-like dendrites were obtained in this cathodic potential range. However, the electrodeposition process between 220 and 266.67 s corresponded to the cathodic potential response between -1210 and -1230 mV vs. Ag/AgCl, and the growth of dendrites in the spear-like form was expected in this cathodic potential range. Actually, it can be assumed that a cathodic potential of -1220 mV vs. Ag/AgCl separating the end of the descending part and the beginning of the plateau of the limiting diffusion current density at the polarization curve for this Sn system [21] represents a critical cathodic potential at which transformation of the dendrite growth from the fern-like to the spear-like shapes occurs. On the other hand, the spear-like part was considerably longer than the fern-like part in the dendrite produced with an amount of the electricity of 400 mC (Fig. 2d). The electrodeposition process between 200 and 400 mC corresponded to the cathodic potential response between -1140 and -1210 mV vs. Ag/AgCl, in which formation of the spear-like dendrites occurs (Fig. 5).

Structural analysis

In the previous section, it is shown that morphology of galvanostatically synthesized Sn dendritic particles strongly depended on

the amount of the passed electricity, and was determined by the chronopotentiometry response. In order to establish whether the chronopotentiometry response also affects a crystal structure of the particles, and hence to establish the existence of correlation between the morphology and structure of the Sn dendrites, XRD analysis of the synthesized particles was done.

Figure 6 shows the XRD patterns recorded for the Sn particles produced at a current density of -3 mA cm $^{-2}$ with amounts of the electricity of 200 and 400 mC, and the corresponding Sn JCPDS standard (04-0673). Comparing the recorded diffraction peaks with those for the standard, it is clear that only Sn diffraction peaks were identified, confirming electrocrystallization of tin in the body-centered tetragonal (bcc) type of crystal lattice [3, 21].

The preferred orientation of Sn particles was estimated from the XRD data by the determination of “Texture Coefficient” ($TC(hkl)$) and “Relative Texture Coefficient” ($RTC(hkl)$). This way enables a precise estimation of the preferred orientation at the semi-quantitative level, and it was widely used for the estimation of the preferred orientation of powder particles in the last time [21, 35–40]. The procedure for the determination of the preferred orientation on this way is given in the Appendix. In the case of Sn, since sixteen (16) diffraction peaks are under consideration, the $RTC(hkl)$ values larger than 6.25% indicated the existence of the preferred orientation in the particles. Simultaneously, the values of $TC(hkl)$ coefficients larger than 1 indicate the existence of preferred orientation [40].

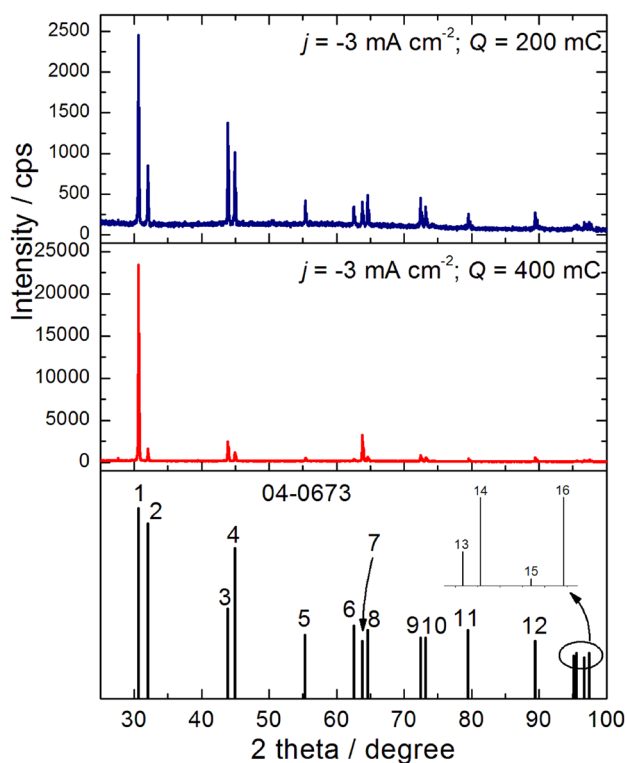


Fig. 6 The X-ray diffraction (XRD) patterns obtained for Sn particles electrodeposited at a current density of -3 mA cm^{-2} with amounts of the electricity of 200 and 400 mC, and Sn standard (04–0673): 1–(200), 2–(101), 3–(220), 4–(211), 5–(301), 6–(112), 7–(400), 8–(321), 9–(420), 10–(411), 11–(312), 12–(431), 13–(103), 14–(332), 15–(440), and 16–(521) crystal planes

The values of $TC(hkl)$ and $RTC(hkl)$ coefficients calculated for the galvanostatically produced particles at a current density of -3 mA cm^{-2} with 200 and 400 mC amounts of the electricity are given in Table 1.

Following $RTC(hkl)$ coefficients, Sn crystallites in the fern-like dendrites produced at -3 mA cm^{-2} with 200 mC amount of the electricity were predominantly oriented in (440),(220) crystal planes. In these dendritic particles, the degree of the preferred orientation changed in the following row: (440) > (220) > (103) > (521) > (400) > (420) (Table 1). In the dendrites with prismatic ends and the spear-like dendrites produced with 400 mC amount of the electricity, the predominant orientation of Sn crystallites was observed in (400),(200) crystal planes. The preferred orientation of these particles changed in the following row: (400) > (200) > (440) > (220).

The similar estimation of the preferred orientation was also obtained by analysis of $TC(hkl)$ coefficients. The preferred orientation of the fern-like dendrites synthesized with an amount of the electricity of 200 mC changed in the following row: (440) > (220) > (103) > (521) > (400) > (420) > (200) > (301) > (321) > (332) > (411) > (431). For the particles obtained after spent amount of the electricity of 400 mC (the dendrites with prismatic ends and the spear-like dendrites), the preferred orientation changed in the following row: (400) > (200) > (440).

The XRD patterns obtained for Sn particles produced potentiostatically at cathodic potentials of $-1200, -1270,$ and $-1600 \text{ mV vs. Ag/AgCl}$, together with the Sn standard,

Table 1 Texture calculations for Sn particles produced at j of -3.0 mA cm^{-2} with amounts of the electricity of 200 and 400 mC. R , intensity of the diffraction peak; TC , texture coefficient; RTC , relative texture coefficient. 200–200 mC; 400–400 mC; s–Sn standard

Plane (hkl)	$R/\%$		$R_s/\%$	TC		$RTC/\%$	
	R_{200}	R_{400} [21]		TC_{200}	TC_{400} [21]	RTC_{200}	RTC_{400} [21]
200	26.6	64.3	22.2	1.20	2.89	5.49	22.1
101	9.19	4.49	20.0	0.46	0.22	2.11	1.72
220	14.9	6.76	7.57	1.97	0.89	9.02	6.85
211	10.9	3.23	16.5	0.66	0.20	3.02	1.50
301	4.52	1.34	3.79	1.19	0.35	5.45	2.71
112	3.78	1.05	5.12	0.74	0.20	3.39	1.57
400	4.39	8.92	2.90	1.51	3.08	6.91	23.6
321	5.29	1.71	4.45	1.19	0.38	5.45	2.94
420	4.88	2.35	3.34	1.46	0.70	6.68	5.40
411	3.72	1.62	3.34	1.11	0.48	5.08	3.72
312	2.82	1.14	4.45	0.63	0.26	2.88	1.96
431	2.95	0.85	2.90	1.02	0.29	4.67	2.25
103	1.16	0.38	0.67	1.73	0.57	7.92	4.40
332	1.32	0.43	1.11	1.19	0.39	5.45	2.99
440	1.86	0.62	0.44	4.23	1.40	19.4	10.7
521	1.72	0.80	1.11	1.55	0.72	7.08	5.50

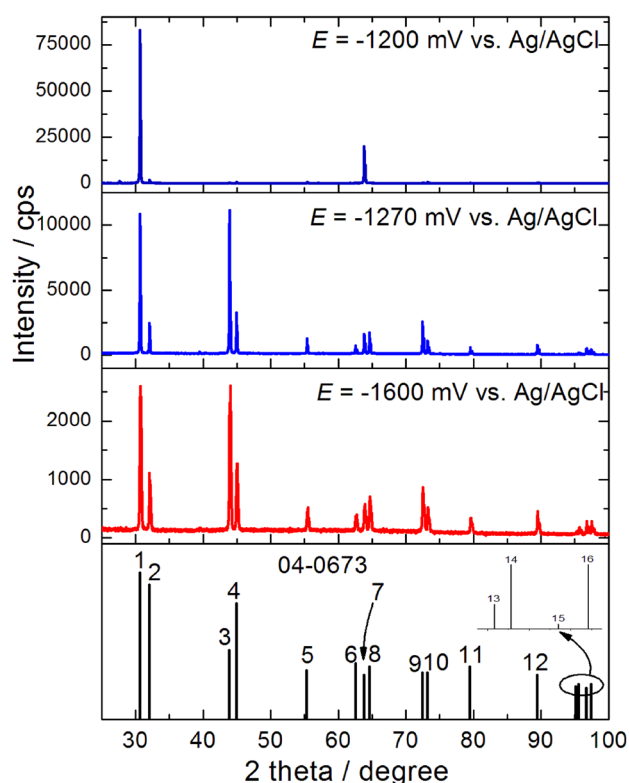


Fig. 7 The X-ray diffraction (XRD) patterns obtained for Sn particles electrodeposited at cathodic potentials of -1200 , -1270 , and -1600 mV vs. Ag/AgCl, and Sn standard (04–0673): 1–(200), 2–(101), 3–(220), 4–(211), 5–(301), 6–(112), 7–(400), 8–(321), 9–(420), 10–(411), 11–(312), 12–(431), 13–(103), 14–(332), 15–(440), and 16–(521) crystal planes

are shown in Fig. 7. Similar to the galvanostatically synthesized particles, only diffraction peaks of Sn were identified confirming the belonging of Sn to the body-centered tetragonal type of crystal lattice. The values of $TC(hkl)$ and $RTC(hkl)$ coefficients calculated for these particles are given in Table 2. Since diffraction peaks for (200) and (400) crystal planes were only identified in the particles produced at -1200 mV vs. Ag/AgCl, the $TC(hkl)$ and $RTC(hkl)$ coefficients for these particles were not determined.

Analysis of $RTC(hkl)$ coefficients given in Table 2 showed that the preferred orientation of the fern-like dendrites produced at -1270 mV vs. Ag/AgCl changed as follows: $(220) > (440) > (420) > (400) > (200)$. For the fern-like dendrites produced at -1600 mV vs. Ag/AgCl, the following row of crystal planes was obtained: $(440) > (220) > (420) > (521) > (400)$. As regards the estimation of the preferred orientation of these fern-like dendrites by analysis of $TC(hkl)$ coefficients, the following rows of crystal planes were observed: $(220) > (440) > (420) > (400) > (200)$ for the fern-like dendrites synthesized at -1270 mV vs. Ag/AgCl, and $(440) > (220) > (420) > (521) > (400) > (103) > (332) > (321) > (411) > (431) > (301)$ for those synthesized at -1600 mV vs. Ag/AgCl. It is necessary to note that the estimation of the preferred orientation of very branchy fern-like dendrites by application of $TC(hkl)$ coefficients was less sensitive relative to the application of $RTC(hkl)$ coefficients. It is manifested by the preferred orientation of the Sn particles produced potentiostatically at -1600 mV vs. Ag/AgCl and galvanostatically at -3 mA cm^{-2} with 200 mC in larger number of crystal planes by analysis of $TC(hkl)$ than $RTC(hkl)$ coefficients.

Table 2 Texture calculations for Sn particles produced at E of -1270 and -1600 mV vs. Ag/AgCl. R , intensity of the diffraction peak; TC , texture coefficient; RTC , relative texture coefficient. $1270 - E = -1270$ mV vs. Ag/AgCl; $1600 - E = -1600$ mV vs. Ag/AgCl; s – Sn standard

Plane (hkl)	$R/\%$		$R_s/\%$	TC		$RTC/\%$	
	R_{1270}	R_{1600}		TC_{1270}	TC_{1600}	RTC_{1270}	RTC_{1600}
200	27.5	20.2	22.2	1.24	0.91	6.84	3.83
101	6.29	8.67	20.0	0.31	0.43	1.71	1.81
220	28.3	20.3	7.57	3.74	2.68	20.6	11.3
211	8.25	9.94	16.5	0.50	0.60	2.76	2.52
301	3.21	4.05	3.79	0.85	1.07	4.69	4.50
112	1.91	3.07	5.12	0.37	0.60	2.04	2.52
400	4.09	4.52	2.90	1.41	1.56	7.77	6.56
321	4.41	5.53	4.45	0.99	1.24	5.46	5.22
420	6.53	6.75	3.34	1.96	2.02	10.8	8.50
411	2.78	4.07	3.34	0.83	1.22	4.58	5.13
312	1.49	2.66	4.45	0.33	0.60	1.82	2.52
431	1.99	3.51	2.90	0.69	1.21	3.80	5.09
103	0.28	0.88	0.67	0.42	1.31	2.32	5.51
332	0.51	1.45	1.11	0.46	1.31	2.54	5.51
440	1.35	2.22	0.44	3.07	5.05	16.9	21.2
521	1.08	2.18	1.11	0.97	1.96	5.37	8.28

Anyway, it is clear that there is a strong correlation between the morphology and structure of synthesized Sn dendrites. In the fern-like dendrites, Sn crystallites were predominantly oriented in (220),(440) crystal planes. With a contribution of orientation of Sn crystallites in these planes between 28.4% (for the particles obtained at -3 mA cm^{-2} with 200 mC) and 37.5% (for those obtained at $-1270 \text{ mV vs. Ag/AgCl}$) relative to all other crystal planes, it is clear that the fern-like dendrites possessed the strong (220),(440) preferred orientation. In the spear-like dendrites and the dendrites with prismatic branches obtained at -3 mA cm^{-2} with 400 mC, Sn crystallites were predominantly oriented in (200),(400) crystal planes, with a share of 45.7% in these planes relative to all other crystal planes. Taking into account the fact that Sn crystallites in the spear-like dendrites and the dendrites with prismatic branches obtained potentiostatically at $-1200 \text{ mV vs. Ag/AgCl}$ were only oriented in (200),(400) crystal planes, it is clear that these shapes of Sn dendrites possessed the strong (200),(400) preferred orientation.

General discussion of the presented results

The comprehensive survey of electrolysis conditions and morphological and structural characteristics of obtained tin dendritic particles is given in Table 3.

The analysis data given in Table 3 confirms the strong correlation among chronopotentiometry response, morphology, and structure of electrolytically formed Sn dendritic particles. With the cathodic potential (chronopotentiometry) response around $-1200 \text{ mV vs. Ag/AgCl}$, the spear-like and the dendrites with prismatic ends with the predominant (200),(400) preferred orientation were

formed. The chronopotentiometry responses above this value, i.e., between the -1210 and $-1740 \text{ mV vs. Ag/AgCl}$, give the fern-like dendrites with Sn crystallites predominantly oriented in (220),(440) crystal planes.

The strong correlation between the morphology and structure of Sn dendrites can be explained by various rates of growth on various crystal planes caused by their various surface energies [41]. For bcc type of crystal lattice, the values of surface energy (γ) follow a trend: $\gamma(110) < \gamma(100) < \gamma(111)$ [42]. This trend has as a consequence the electrodeposition rates on (110), and hence on (220) and (440) crystal planes which are smaller than on all other crystal planes. During electrolysis process, these planes survive constructing an interior of stalk and branches in the fern-like dendrites, and for that reason, these planes are denoted as slow-growing crystal planes. All other crystal planes can be denoted as fast-growing crystal planes, and they disappear during growth process. The orientation of crystallites in all other crystal planes originates from crystal growth at tips and angles of growing dendrites. With a chronopotentiometry response of about $-1200 \text{ mV vs. Ag/AgCl}$, electrodeposition rate is low enough that a crystal plane with the higher surface energy ((100), and hence (200),(400)) can survive a crystal growth constructing the spear-like and the dendrites with the prismatic branches of almost monocrystalline character of this preferred orientation.

On the basis of the presented results, it is clear that the analysis of chronopotentiometry response obtained during the production of metal powders by galvanostatic regime of electrolysis represents good diagnostic criteria for a prediction of shapes of powder particles (in this case, Sn) of desired morphological and structural characteristics.

Table 3 The parameters of electrodeposition, the types of morphology, and crystal structure (preferred orientation) of Sn particles produced under various conditions of electrolysis

The electrodeposition parameters	Type of morphology of Sn particles	The crystal structure (preferred orientation) of Sn particles	
		TC(hkl)	RTC(hkl)%
$j = -3 \text{ mA cm}^{-2}$; $Q = 200 \text{ mC}$; $E = (-1210 \div -1740) \text{ mV vs. Ag/AgCl}$	The fern-like dendrites	(440) > (220) > (103) > (521) > (400) > (420) > (200) > (301) > (321) > (332) > (411) > (431)	(440) > (220) > (103) > (521) > (400) > (420)
$j = -3 \text{ mA cm}^{-2}$; $Q = 400 \text{ mC}$; $E = (-1140 \div -1210) \text{ mV vs. Ag/AgCl}$	The spear-like dendrites and dendrites with prismatic ends	(400) > (200) > (440)	(400) > (200) > (440) > (220)
$E = -1270 \text{ mV vs. Ag/AgCl}$	The fern-like dendrites	(220) > (440) > (420) > (400) > (200)	(220) > (440) > (420) > (400) > (200)
$E = -1600 \text{ mV vs. Ag/AgCl}$	The fern-like dendrites	(440) > (220) > (420) > (521) > (400) > (103) > (332) > (321) > (411) > (431) > (301)	(440) > (220) > (420) > (521) > (400)
$E = -1200 \text{ mV vs. Ag/AgCl}$	The spear-like dendrites and dendrites with prismatic ends	(200) > (400)	

Conclusion

Sn dendrites were produced by galvanostatic regime of electrolysis from the alkaline hydroxide electrolyte at a current density of -3 mA cm^{-2} , with amounts of the electricity of 200 and 400 mC. Morphology and structure of the produced particles were characterized by scanning electron microscopy (SEM) and X-ray diffraction (XRD) techniques, respectively. The chronopotentiometry response recorded at the given current density and morphological and structural analyses of Sn particles produced by potentiostatic regime of electrolysis at the cathodic potentials which corresponded to the chronopotentiometry curve were used to explain the morphology and structure of galvanostatically obtained particles with various amounts of the electricity. On the basis of the obtained results, it follows:

Morphology of Sn dendrites strongly depended on the amount of spent electricity, and it was determined by the value of cathodic potential (chronopotentiometry) response reached during electrolysis process. The fern-like dendrites were predominately formed with an amount of the electricity of 200 mC, and the chronopotentiometry response in the $-1210 \div -1740 \text{ mV}$ vs. Ag/AgCl range corresponded to the formation of this dendrite shape. The spear-like dendrites and those with prismatic branches (or ends) were formed with spent amount of the electricity of 400 mC. The chronopotentiometry response of about -1200 mV vs. Ag/AgCl was responsible for the formation of these particles.

The strong correlation among chronopotentiometry response, morphology, and structure of Sn dendritic particles was established. The fern-like dendrites exhibited the strong (220),(440) preferred orientation, while the spear-like and the dendrites with prismatic branches showed the strong (200),(400) preferred orientation.

The chronopotentiometry response obtained during the application of galvanostatic regime of electrolysis represents important diagnostic criteria enabling a control of morphology and structure of electrolytically produced Sn dendrites.

Appendix 1

Determination of the “Texture Coefficient” $TC(hkl)$ and the “Relative Texture Coefficient” $RTC(hkl)$ by analysis of the XRD data

The ratio of reflection intensity (hkl) to the sum of all intensities of the recorded reflections, $R(hkl)$, (in %) is given by Eq. (1) [39]:

$$R(hkl) = \frac{I(hkl)}{\sum_i^{16} I(h_i k_i l_i)} \times 100 \quad (1)$$

where $I(hkl)$ is a reflection intensity (hkl) plane, in cps, and $\sum_i^{16} I(h_i k_i l_i)$ is the sum of all intensities of the recorded reflections, in cps, for the powder being considered (in the case of Sn, it is sixteen).

The “Texture Coefficient,” $TC(hkl)$, for every (hkl) reflection is defined by Eq. (2):

$$TC(hkl) = \frac{R(hkl)}{R_s(hkl)} \quad (2)$$

where $R_s(hkl)$ is defined in the same way as given by Eq. (2), but is related to the standard for metal under consideration. This coefficient gives the accurate quantitative information about the absolute reflection intensity.

Finally, the “Relative Texture Coefficient” $RTC(hkl)$, (in %) is defined by Eq. (3):

$$RTC(hkl) = \frac{TC(hkl)}{\sum_i^{16} TC(h_i k_i l_i)} \times 100 \quad (3)$$

The $RTC(hkl)$ coefficient defines the reflection intensity (hkl) relative to the standard (included in the TC values).

Funding This work was supported by the Ministry of Education, Science and Technological Development of the Republic of Serbia (RS) (Grant Nos. 451-03-68/2022-14/200026 and 451-03-9/2022-14/200017) and Science Fund of RS (Grant No. AdCatFC: 7739802).

References

1. Tin powder – production and applications. <https://nanografi.com/blog/tin-sn-powder/>. Accessed 07 Oct 2022
2. Rudnik E (2013) Effect of anions on the electrodeposition of tin from acidic gluconate baths. *Ionics* 19:1047–1059. <https://doi.org/10.1007/s11581-012-0819-4>
3. Wang Z, Ru J, Hua Y, Bu J, Geng X, Zhang W (2021) Electrodeposition of Sn powders with pyramid chain and dendrite structures in deep eutectic solvent: roles of current density and SnCl_2 concentration. *J Solid State Electrochem* 25:1111–1120. <https://doi.org/10.1007/s10008-020-04894-7>
4. Zhang LP, Zhao YY (2017) Particle size distribution of tin powder produced by centrifugal atomisation using rotating cups. *Powder Technol* 318:62–67. <https://doi.org/10.1016/j.powtec.2017.05.038>
5. Chee SS, Lee JH (2012) Reduction synthesis of tin nanoparticles using various precursors and melting behavior. *Electron Mater Lett* 8:587–593. <https://doi.org/10.1007/s13391-012-2086-y>
6. Zou CD, Gao YL, Yang B, Zhai QJ (2010) Size-dependent melting properties of Sn nanoparticles by chemical reduction synthesis. *Trans Nonferrous Met Soc China* 20:248–253. [https://doi.org/10.1016/S1003-6326\(09\)60130-8](https://doi.org/10.1016/S1003-6326(09)60130-8)
7. Chee SS, Lee JH (2012) Synthesis of tin nanoparticles through modified polyol process and effects of centrifuging and drying on nanoparticles. *Trans Nonferrous Met Soc China* 22:707–711. [https://doi.org/10.1016/S1003-6326\(12\)61791-9](https://doi.org/10.1016/S1003-6326(12)61791-9)

8. Qiu L, Pol VG, Calderon-Moreno J, Gedanken A (2005) Synthesis of tin nanorods via a sonochemical method combined with a polyol process. *Ultrason Sonochem* 12:243–247. <https://doi.org/10.1016/j.ultsonch.2004.02.001>
9. Dong J, Wu F, Han Q, Qi J, Gao W, Wang Y, Li T, Yang Y, Sun M (2020) Electrochemical synthesis of tin plasmonic dendritic nanostructures with SEF capability through in situ replacement. *RSC Adv* 10:36042–36050. <https://doi.org/10.1039/D0RA06483A>
10. Riviello AE Jr, Young D, Sebba F (1994) A novel method for production of finely divided tin metal powders. *Powder Technol* 78:19–24. [https://doi.org/10.1016/0032-5910\(93\)02767-5](https://doi.org/10.1016/0032-5910(93)02767-5)
11. Amiri M, Nouhi S, Azizian-Kalandaragh Y (2015) Facile synthesis of silver nanostructures by using various deposition potential and time: a nonenzymatic sensor for hydrogen. *Mater Chem Phys* 155:129–135. <https://doi.org/10.1016/j.matchemphys.2015.02.009>
12. Popov KI, Djokić SS, Nikolić ND, Jović VD (2016) Morphology of electrochemically and chemically deposited metals. Springer New York USA 1–368. <https://doi.org/10.1007/978-3-319-26073-0>
13. Popov KI, Pavlović MG, Jovičević JN (1989) Morphology of tin powder particles obtained in electrodeposition on copper cathode by constant and square-wave pulsating overpotential from Sn(II) alkaline solution. *Hydrometallurgy* 23:127–137. [https://doi.org/10.1016/0304-386X\(89\)90023-6](https://doi.org/10.1016/0304-386X(89)90023-6)
14. Kim TH, Hong KS, Sohn DR, Kim MJ, Nam DH, Cho EA, Kwon HS (2017) One-step synthesis of multilayered 2D Sn nanodendrites as a high-performance anode material for Na-ion batteries. *J Mater Chem A* 5:20304–20315. <https://doi.org/10.1039/C7TA06469A>
15. Rudnik E, Włoch G (2013) Studies on the electrodeposition of tin from acidic chloride–gluconate solutions. *Appl Surf Sci* 265:839–849. <https://doi.org/10.1016/j.apsusc.2012.11.130>
16. He A, Liu Q, Ivey DG (2008) Electrodeposition of tin: a simple approach. *J Mater Sci: Mater Electron* 19:553–562. <https://doi.org/10.1007/s10854-007-9385-3>
17. Shin HC, Dong J, Liu M (2003) Nanoporous structures prepared by an electrochemical deposition process. *Adv Mater* 15:1610–1614. <https://doi.org/10.1002/adma.200305160>
18. Khabazian S, Sanjabi S, Tonti D (2020) Electrochemical growth of two-dimensional tin nano-platelet as high-performance anode material in lithium-ion batteries. *J Ind Eng Chem* 84:120–130. <https://doi.org/10.1016/j.jiec.2019.12.027>
19. Azpeitia LA, Gervasi CA, Bolzan AE (2019) Electrochemical aspects of tin electrodeposition on copper in acid solutions. *Electrochim Acta* 298:400–412. <https://doi.org/10.1016/j.electacta.2018.12.040>
20. Low CTJ, Walsh FC (2008) The influence of a perfluorinated cationic surfactant on the electrodeposition of tin from a methanesulfonic acid bath. *J Electroanal Chem* 615:91–102. <https://doi.org/10.1016/j.jelechem.2007.11.031>
21. Nikolić ND, Lović JD, Maksimović VM, Živković PM (2022) Morphology and structure of electrolytically synthesized tin dendritic nanostructures. *Metals* 12:1201. <https://doi.org/10.3390/met12071201>
22. Wranglen G (1960) Dendrites and growth layers in the electrocrystallization of metals. *Electrochim Acta* 2:130–146. [https://doi.org/10.1016/0013-4686\(60\)87010-7](https://doi.org/10.1016/0013-4686(60)87010-7)
23. Walsh FC, Low CTJ (2016) A review of developments in the electrodeposition of tin. *Surf Coat Technol* 288:79–94. <https://doi.org/10.1016/j.surfcoat.2015.12.081>
24. Lodge AW, Hasan MM, Bartlett PN, Beanland R, Hector AL, Kashtiban RJ, Levason W, Reid G, Sloan J, Smith DC, Zhang W (2018) Electrodeposition of tin nanowires from a dichloromethane based electrolyte. *RSC Adv* 8:24013–24020. <https://doi.org/10.1039/C8RA03183E>
25. Santato C, Lopez CM, Choi K-S (2007) Synthesis and characterization of polycrystalline Sn and SnO₂ films with wire morphologies. *Electrochem Commun* 9:1519–1524. <https://doi.org/10.1016/j.elecom.2007.02.006>
26. Wang Z, Ru J, Hua Y, Wang D, Bu J (2020) Morphology-controlled preparation of Sn powders by electrodeposition in deep eutectic solvent as anodes for lithium ion batteries. *J Electrochem Soc* 167:082504. <https://doi.org/10.1149/1945-7111/ab8824>
27. Cao X, Xu L, Wang C, Li S, Wu D, Shi Y, Liu F, Xue X (2020) Electrochemical behavior and electrodeposition of Sn coating from choline chloride–urea deep eutectic solvents. *Coatings* 10:1154. <https://doi.org/10.3390/coatings10121154>
28. Liu D, Groult H, Gaillon L, Rizzi C, Soulmi N, Julien CM, Briot E, Krulic D (2015) Tunable electrodeposition of Sn and Sn-based alloys using ionic liquids. *J Solid State Electrochem* 19:2517–2532. <https://doi.org/10.1007/s10008-015-2809-8>
29. Hsu CH, Yang CH, Wang YC, Chang JK (2014) Nanostructured tin electrodeposited in ionic liquid for use as an anode for Li-ion batteries. *J Mater Chem A* 2:16547–16553. <https://doi.org/10.1039/C4TA03709J>
30. Elbasiony AMR, Zein El Abedin S, Endres F (2014) Electrochemical synthesis of freestanding tin nanowires from ionic liquids. *J Solid State Electrochem* 18:951–957. <https://doi.org/10.1007/s10008-013-2340-8>
31. Elbasiony AM, Prowald A, Abedin SZE, Endres F (2022) Electrochemical synthesis of nanowires and macroporous CuSn alloy from ionic liquids. *J Solid State Electrochem* 26:783–789. <https://doi.org/10.1007/s10008-021-05109-3>
32. Winand R (1994) Electrodeposition of metals and alloys—new results and perspectives. *Electrochim Acta* 39:1091–1105. [https://doi.org/10.1016/0013-4686\(94\)E0023-S](https://doi.org/10.1016/0013-4686(94)E0023-S)
33. Nikolić ND, Živković PM, Pavlović MG, Baščarević Z (2019) Overpotential controls a morphology of electrolytically produced copper dendritic forms. *J Serb Chem Soc* 84:1209–1220. <https://doi.org/10.2298/JSC190522066N>
34. Popov KI, Pavlović MG, Maksimović MD, Krstajić S (1978) The comparison of galvanostatic and potentiostatic copper powder deposition on platinum and aluminium electrodes. *J Appl Electrochem* 8:503–514. <https://doi.org/10.1007/BF00610795>
35. Lj A, Pavlović MM, Maksimović VM, Vuković M, Stevanović JS, Bugarin M, Nikolić ND (2017) Comparative morphological and crystallographic analysis of electrochemically- and chemically-produced silver powder particles. *Metals* 7:160. <https://doi.org/10.3390/met7050160>
36. Lj A, Maksimović VM, Baščarević Z, Ignjatović N, Bugarin M, Marković R, Nikolić ND (2019) Influence of the shape of copper powder particles on the crystal structure and some decisive characteristics of the metal powders. *Metals* 9:56. <https://doi.org/10.3390/met9010056>
37. Lj A, Ivanović ER, Maksimović VM, Pavlović MM, Vuković M, Stevanović JS, Nikolić ND (2018) Correlation between crystal structure and morphology of potentiostatically electrodeposited silver dendritic nanostructures. *Trans Nonferrous Met Soc China* 28:1903–1912. [https://doi.org/10.1016/S1003-6326\(18\)64835-6](https://doi.org/10.1016/S1003-6326(18)64835-6)
38. Nikolić ND, Lj A, Ivanović ER, Maksimović VM, Baščarević Z, Ignjatović N (2019) Comparative morphological and crystallographic analysis of copper powders obtained under different electrolysis conditions. *Trans Nonferrous Met Soc China* 29:1275–1284. [https://doi.org/10.1016/S1003-6326\(19\)65034-X](https://doi.org/10.1016/S1003-6326(19)65034-X)
39. Nikolić ND, Maksimović VM, Lj A (2021) Correlation of morphology and crystal structure of metal powders produced by electrolysis processes. *Metals* 11:859. <https://doi.org/10.3390/met11060859>
40. Berube LPh, Esperance GL (1989) A quantitative method of determining of the degree of texture of zinc electrodeposits. *J Electrochem Soc* 136:2314–2315. <https://doi.org/10.1149/1.2097318>
41. Bockris JOM, Reddy AKN, Gamboa-Aldeco ME (2000) Modern electrochemistry 2A: fundamentals of electrochemistry. Kluwer Academic/Plenum Publishers, New York, Boston, Dordrecht, London, Moscow

42. Wang SG, Tian EK, Lung CW (2000) Surface energy of arbitrary crystal plane of bcc and fcc metals. *J Phys Chem Solids* 61:1295–1300. [https://doi.org/10.1016/S0022-3697\(99\)00415-1](https://doi.org/10.1016/S0022-3697(99)00415-1)

Publisher's Note Springer Nature remains neutral with regard to jurisdictional claims in published maps and institutional affiliations.

Springer Nature or its licensor (e.g. a society or other partner) holds exclusive rights to this article under a publishing agreement with the author(s) or other rightsholder(s); author self-archiving of the accepted manuscript version of this article is solely governed by the terms of such publishing agreement and applicable law.